Simulated versus observed patterns of warming over the extratropical Northern Hemisphere continents during the cold season

John M. Wallace[a,1], Qiang Fu[a,b], Brian V. Smoliak[a], Pu Lin[a], and Celeste M. Johanson[a]

[a]Department of Atmospheric Sciences, University of Washington, Seattle, WA 98195-1640; and [b]College of Atmospheric Sciences, Lanzhou University, Lanzhou 730000, China

Edited by Robert E. Dickinson, The University of Texas at Austin, Austin, TX, and approved July 9, 2012 (received for review March 26, 2012)

A suite of the historical simulations run with the Intergovernmental Panel on Climate Change Fourth Assessment Report (IPCC AR4) models forced by greenhouse gases, aerosols, stratospheric ozone depletion, and volcanic eruptions and a second suite of simulations forced by increasing CO_2 concentrations alone are compared with observations for the reference interval 1965–2000. Surface air temperature trends are disaggregated by boreal cold (November-April) versus warm (May-October) seasons and by high latitude northern (N: 40°–90 °N) versus southern (S: 60 °S–40 °N) domains. A dynamical adjustment is applied to remove the component of the cold-season surface air temperature trends (over land areas poleward of 40 °N) that are attributable to changing atmospheric circulation patterns. The model simulations do not simulate the full extent of the wintertime warming over the high-latitude Northern Hemisphere continents during the later 20th century, much of which was dynamically induced. Expressed as fractions of the concurrent trend in global-mean sea surface temperature, the relative magnitude of the dynamically induced wintertime warming over domain N in the observations, the simulations with multiple forcings, and the runs forced by the buildup of greenhouse gases only is 7:2:1, and roughly comparable to the relative magnitude of the concurrent sea-level pressure trends. These results support the notion that the enhanced wintertime warming over high northern latitudes from 1965 to 2000 was mainly a reflection of unforced variability of the coupled climate system. Some of the simulations exhibit an enhancement of the warming along the Arctic coast, suggestive of exaggerated feedbacks.

spatial patterns of warming | climate model diagnostics | dynamically-induced warming | polar amplification

The rate of increase of global-mean surface temperature (GST) in the historical record has been irregular, with rapid warming early in the 20th century, a midcentury hiatus, and a resumption of the warming in 1965, as shown in Fig. 1. The Fourth Assessment Report (AR4) of the Intergovernmental Panel on Climate Change (IPCC) featured a set of historical simulations in which the simulated warming of GST, indicated by the dotted gray curve in Fig. 1, roughly parallels the observed warming during the historical record.

Here, we present results of a detailed comparison between the observed trends and the trends in the AR4 simulations during the reference interval 1965–2000 (1). The climate forcing during this period was characterized by the rapid buildup of greenhouse gases, stratospheric ozone depletion in the Antarctic (and, to a lesser extent, in the Arctic), and three major tropical volcanic eruptions that injected large amounts of sulfur dioxide into the stratosphere, producing aerosols. Prior to 1965, tropospheric aerosol concentrations had been increasing almost everywhere, but by the 1980s they had begun to decrease over North America and Europe in response to tightening air pollution–control regulations. Many of the AR4 historical simulations have representations of these time-varying forcings (1, 2).

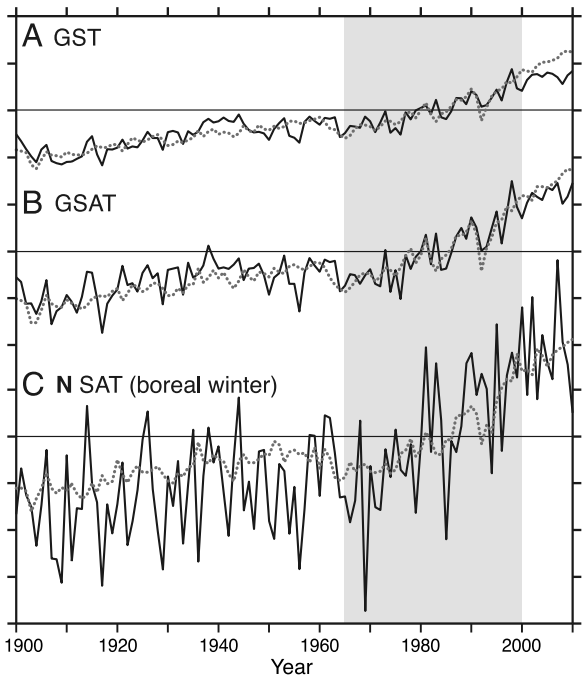

Fig. 1. Observed (solid) and multimodel ensemble mean (MMEM; dotted) temperature anomaly time series with respect to the 1965–2000 reference period (indicated by light gray shading) for: (*A*) annual-mean, global-mean surface temperature (GST); (*B*) annual-mean, global-mean surface air temperature over land (GSAT); and (*C*) boreal cold-season SAT over land averaged poleward of 40 °N (**N** SAT). Tick marks on the abscissa denote 0.5 °C. Observational data based on National Oceanic and Atmospheric Administration (NOAA) merged land-ocean surface temperature analysis (MLOST). Model data based on AR4 historical simulations with ozone depletion and volcanic aerosols. See Tables S1 and S2 for further details.

In way of circulation changes, 1965–2000 was marked by a strong tendency toward the positive polarity of the Northern Hemisphere annular mode (NAM) (3, 4) and a shift (around 1976–1977) toward the warm polarity of the El Niño/Southern Oscillation (ENSO) cycle (5–7), both of which favored increased advection of mild marine air masses over the colder continents poleward of approximately 40 °N during wintertime, resulting

Author contributions: J.M.W. and Q.F. designed research; J.M.W., Q.F., B.V.S., P.L., and C.M.J. performed research; B.V.S., P.L., and C.M.J. analyzed data; and J.M.W., Q.F., B.V.S., and P.L. wrote the paper.

The authors declare no conflict of interest.

This article is a PNAS Direct Submission.

See Commentary on page 14285.

[1]To whom correspondence should be addressed. E-mail: wallace@atmos.washington.edu.

This article contains supporting information online at www.pnas.org/lookup/suppl/doi:10.1073/pnas.1204875109/-/DCSupplemental.

Table 1. Temperature trends for observations and the MMEM of AR4 model historical simulations and 2x CO_2 simulations, partitioned by latitude and season *

	Observations†		AR4 Models			
			Historical simulations†		2x CO_2 simulations‡	
	1965–2000		1965–2000			
	Cold	Warm	Cold	Warm	Cold	Warm
N: 40° N–90° N	1.72 (*1.02*)	0.79	1.34 (*1.06*)	0.84	2.65 (*2.32*)	2.01
S: 60° S–40° N	0.70	0.69	0.65	0.72	1.88	2.02
GSAT (land)	1.03 (*0.80*)	0.72	0.87 (*0.78*)	0.76	2.13 (*2.03*)	2.02
GSST (ocean)	0.35	0.37	0.49	0.46	1.40	1.34
GST	0.57 (*0.49*)	0.48	0.60 (*0.58*)	0.55	1.62 (*1.59*)	1.54

All statistics refer to surface air temperature over land (SAT) except for the bottom two rows, which refer to global-mean sea surface temperature (GSST) and global-mean surface temperature (GST). Dynamically adjusted trends indicated in italics.
*As discussed in text.
†Units are °C per 36 years in observations and historical simulations.
‡Units are °C for CO_2 doubling in the 2x CO_2 simulations.

in a dynamically induced warming trend strong enough to augment the wintertime warming over the Northern Hemisphere as a whole (8–10). Results of numerical experiments suggest that anthropogenic forcing has contributed to the observed circulation changes during this period (11–13) but cannot account for their large amplitude (14).

In this study, the warming is partitioned into dynamically induced and radiatively forced components, and the latter into components associated with the buildup of greenhouse gases alone versus that caused by the other time-varying forcings. Trends for boreal cold and warm seasons (November–April versus May–October) are considered separately. The dynamical contribution to the trend is estimated using the methodology described in *Materials and Methods*.

To get some insight into the relative importance of the contribution of the varying forcings, the trends in the AR4 historical simulations are compared with simulated trends in a suite of runs forced only by a transient doubling of atmospheric CO_2 concentrations, which are prescribed to increase at a rate of 1% per year over a 70-year interval. In the historical runs the forcing includes not only the buildup of greenhouse gases, but also the time-varying loading of tropospheric aerosols, stratospheric ozone depletion, and sulfate aerosols injected into the stratosphere by explosive volcanic eruptions. Results are presented in the next section and discussed in the final section of the paper.

Results

Comparison of Simulated and Observed Trends Dimer In Situ. The first two columns of Table 1 show observed 1965–2000 surface temperature trends separated by land and ocean, by northern (40 °N–90 °N, henceforth referred to as **N**) and southern (60 °S–40 °N, **S**) domains and by cold and warm seasons. More comprehensive statistics based on an array of observational datasets, presented in Table S3, are in close agreement with these results. Averaged over the year and over the globe, surface air temperature over land (GSAT) rose 2.4 times as much as sea surface temperature (GSST; 0.87 °C versus 0.36 °C) during the reference interval. Over land, averaged over the year, the warming over **N** was nearly twice as strong as over **S** (1.25 °C versus 0.69 °C). Within **N**, SAT warmed more than twice as much during the boreal cold season as during the warm season. In contrast, the amount of warming within **S** exhibited little seasonality and was comparable to that in **N** during the warm season (i.e., approximately 0.7 °C over the 36-year interval). The enhancement of the observed warming over the interior of the Northern Hemisphere continents poleward of 40 °N during the boreal cold season is clearly evident in the geographical distribution of the warming, shown in Fig. 2*A*: The meridional profile of the zonally (land only) averaged warming exhibits a pronounced peak centered approximately 60 °N, where the temperature rise exceeded 2 °C.

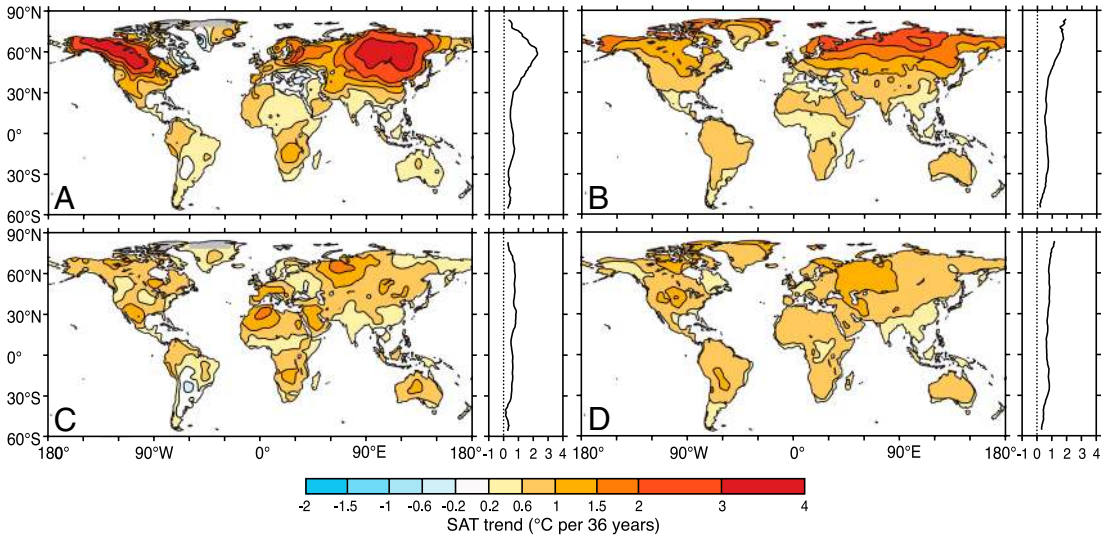

Fig. 2. Maps and zonally averaged meridional profiles showing rates of warming over the historical reference interval 1965–2000 expressed in units of °C per 36 years: (*A*, *B*) boreal cold season; (*C*, *D*) boreal warm season. The left column (*A*, *C*) is based on the NOAA MLOST dataset and the right column (*B*, *D*) is based on the MMEM of AR4 models listed in Table S1.

The corresponding spatial patterns of the simulated trends, as represented by the multimodel ensemble mean (MMEM), and an average over all nine model results after averaging the ensemble runs of each model, are shown in Fig. 2, *Right*. Spatial patterns of simulated trends for the 21 individual model runs are shown in *SI Text* (Fig. S1). In the simulations (Fig. 2*B*), the strongest warming occurs poleward of 65 °N along the coast of the Arctic Ocean, whereas in the observations (Fig. 2*A*) it occurs over the interior of the continents poleward of 40 °N. The observed and simulated trends for the boreal warm season (Fig. 2 *C* and *D*) are both relatively featureless. Despite the differences between the observed and simulated patterns for the boreal cold season, the area-averaged simulated trends summarized in the third and fourth columns of Table 1 are roughly comparable to those from observations. The largest discrepancy is over **N** during the boreal cold season, where the simulated warming is approximately 25% too small. This distinction between observations and simulations is clearly apparent in the time series shown in Fig. 1*C*.

Comparison of the Dynamically Adjusted Trends To investigate the degree to which the enhanced warming over the high-latitude continents during the boreal cold season is attributable to changes in the atmospheric circulation during the reference period, we applied a "dynamical adjustment" to the time series of area-averaged SAT poleward of 40 °N, as described in *Materials and Methods*, for both observations and each of the simulations. The adjustment is based on a longer reference period: 1920–2008. The adjustment was applied only to the boreal cold-season (NDJFMA) temperatures; the dynamical contribution to warm season (MJJASO) was found to be much smaller and is ignored in this paper.

In the summary statistics presented in Table 2, it can be seen that applying the dynamical adjustment to the observations reduces the 1965–2000 trend averaged over **N** during the boreal cold season by 41% (from 1.72 °C to 1.02 °C). The corresponding percentage reduction in the MMEM is 21%. The observed and MMEM-simulated patterns of sea-level pressure (SLP) trends upon which the dynamical adjustment is based are shown in Fig. 3 *A* and *B*. Taking into account the smaller contour interval for the MMEM pattern, it is evident that the observed SLP trends during the interval 1965–2000 were about three times as strong as those in the MMEM simulation.

Fig. 4 shows time series of raw and dynamically adjusted **N** SAT based on observations; the MMEM; a run of the Goddard Institute for Space Studies (GISS) Model ER, which exemplifies the models with small interannual variability; and a run of the Community Climate System Model, version 3 (CCSM3), which exemplifies the runs with large interannual variability. The time series of the MMEM simulation is much smoother than the other curves and its appearance is not substantially changed by the application of the dynamical adjustment to the individual runs that it represents. The individual GISS simulations are also notably deficient in dynamically induced variability whereas the CCSM3 simulations are somewhat hyperactive in this respect. Notwithstanding these differences, the MMEM of the variance of the dynamically induced component of **N** SAT in the historical simulations (0.62 °C^2) is roughly comparable to that in the observations (0.70 °C^2), as assessed from monthly-mean data.

Table 2. Comparison of boreal cold-season statistics between observations, historical simulations, and 2x CO_2 simulations with respect to the SAT rise averaged over N before and after applying the dynamical adjustment

	SAT rise (°C), raw (adjusted)*	R1†	R2‡
Observations	1.72 (*1.02*)	1.94	0.41
Historical simulation MMEM	1.34 (*1.06*)	0.59	0.21
2x CO_2 simulation MMEM	2.65 (*2.32*)	0.24	0.12

*SAT rise statistics are based on the historical reference period 1965–2000 for observations and historical simulations, and on 70 years of output for the 2x CO_2 simulations.

†Ratio of the dynamical contribution to the change in annual-mean GSST (see Table 1).

‡Ratio of the dynamical contribution to the raw, unadjusted SAT change.

Trends in CO_2-Doubling Simulations The AR4 historical simulations examined in the previous two sections incorporate forcings from greenhouse gases and aerosols as well as the impacts of volcanic eruptions and stratospheric ozone depletion. To aid in the interpretation of these results, we show in Fig. 5 the warming trends simulated in experiments forced only by the buildup of atmospheric CO_2, prescribed to increase at a rate of 1% per year, which were conducted with several of the models in the CMIP3 dataset. The SAT and SLP changes are estimated for a 70-year interval over which the CO_2 concentration doubles. The rates of warming in these simulations are not directly comparable with those discussed in previous sections, but the seasonal and **N**/**S** breakdowns of the changes and the relative importance of the dynamical contribution can be compared.

From the similarity between the spatial pattern of the warming in the simulations forced by transient CO_2 doubling alone (Fig. 5) and the pattern in the 1965–2000 simulations with the multiple forcings (Fig. 2) it can be concluded that the additional forcings included in the AR4 historical simulations (i.e., stratospheric ozone depletion, tropospheric aerosols, and stratospheric aerosols resulting from volcanic eruptions) do not materially change the spatial patterns of the trends in the 2x CO_2 MMEM simula-

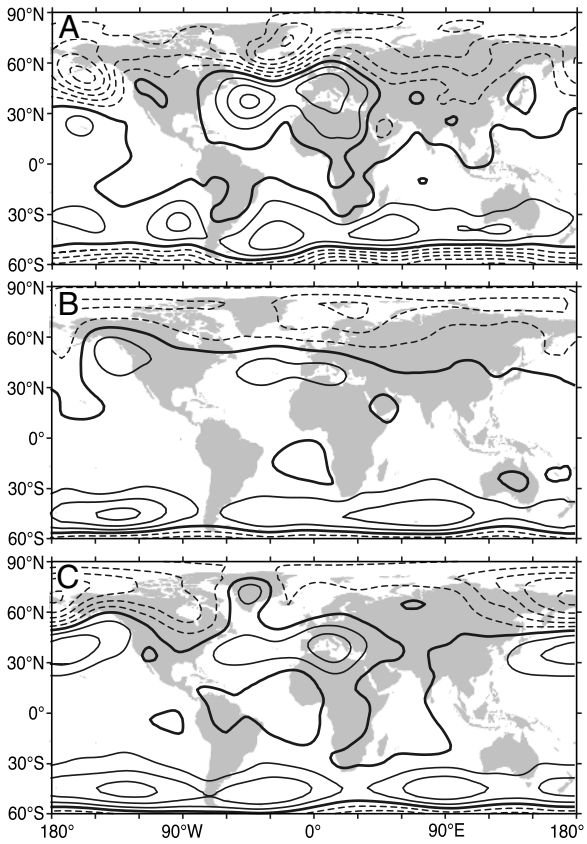

Fig. 3. Boreal cold-season SLP trends for: (*A*) observations 1965–2000 (contour interval, 1 hPa per 36 years); (*B*) MMEM of AR4 historical simulations 1965–2000 (contour interval, 0.5 hPa per 36 years); and (*C*) MMEM of AR4 2x CO_2 simulations (units are hPa for CO_2 doubling; contour interval, 0.5 hPa). Negative contours, dashed; zero contour, bold. MMEM based on AR4 models listed in Table S1.

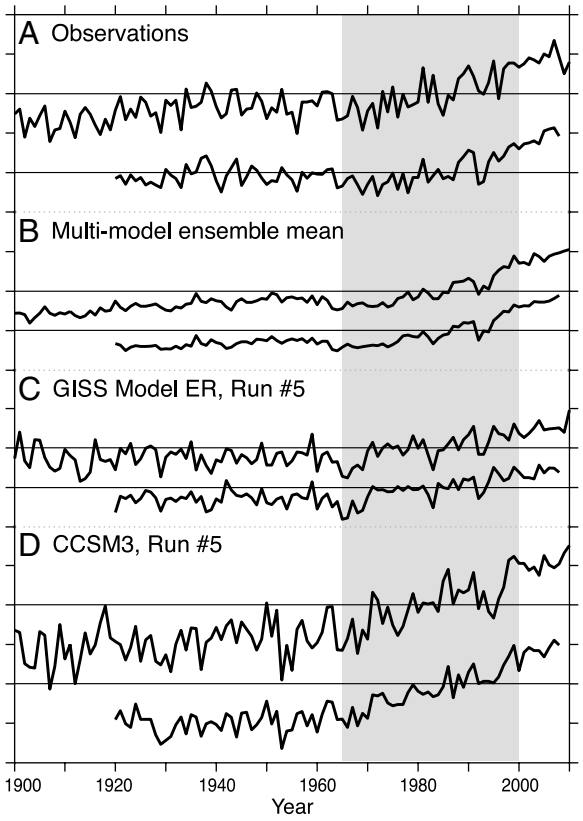

Fig. 4. Raw (*Upper*) and dynamically adjusted (*Lower*) annual-mean **N** SAT for: (*A*) observations; (*B*) MMEM; (*C*) GISS model ER run #5; and (*D*) CCSM3 run #5. Each tick mark on the abscissa indicates 1 °C.

tion. Given that CO_2 concentration in these experiments is prescribed to be spatially uniform, the polar amplification signal along the coast of the Arctic Ocean during the boreal cold season must be occurring in response to feedbacks that are common to the simulations shown in Figs. 2 and 5.

The spatial pattern of SLP changes in the MMEM 2x CO_2 simulation in Fig. 3*C*, is qualitatively similar to the SLP changes in the historical simulations shown in Fig. 3*B*. To compare the magnitudes of the two patterns it is perhaps most meaningful to scale them per degree of annual-mean GSST using the values for the historical runs and 2x CO_2 runs listed in Table 1 because GSST is not affected by the size of the dynamical adjustment and is not strongly seasonally dependent. Scaled in this manner, the SLP changes are more than a factor of two larger in the historical runs than in the 2x CO_2 runs. Similarly, the scaled SAT changes attributable to the dynamical contribution in **N** are slightly more than a factor of two larger in the historical runs than in the 2x CO_2 runs (column R1, Table 2). A more local measure of the strength of the dynamical response in the 2x CO_2 runs relative to that in the historical runs is the percentage of the warming over **N** during the cold season that is attributable to the dynamical contribution, listed as R2 in Table 2: 12% in the 2x CO_2 MMEM simulation, as compared with 21% in the historical MMEM simulation that include forcings other than greenhouse gases. By all three measures, the simulated dynamical response to rising CO_2 concentrations alone is less than half as large as the simulated response to the suite of radiative forcing agents included in the historical simulations.

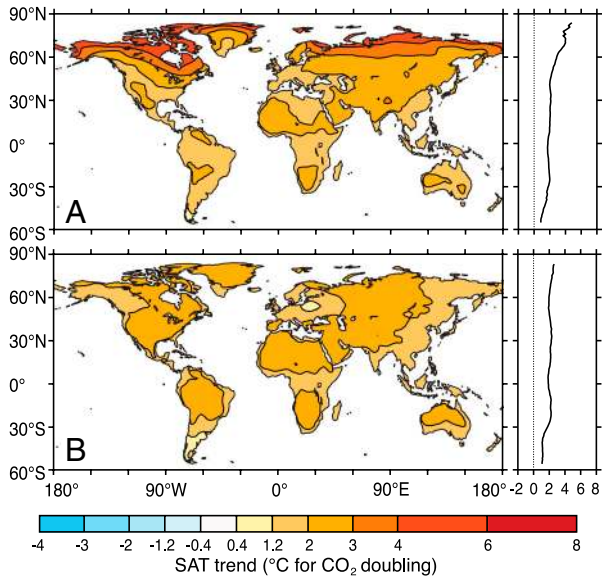

Fig. 5. Maps and zonally averaged meridional profiles showing rates of warming for 2x CO_2 simulations based on the MMEM of AR4 models listed in Table S1: (*A*) boreal cold season, and (*B*) boreal warm season. Units are °C for CO_2 doubling.

Discussion

Although the models used in the AR4 historical climate simulations replicate the observed rise in global-mean surface air temperature during the 1965–2000 reference interval, the spatial patterns of warming exhibit some notable departures from the observations during the boreal cold season. A notable discrepancy is the failure of the models to simulate the full extent of the accelerated warming over the interior of the Northern Hemisphere continents centered at approximately 60 °N, which ranged up to as much as 3 °C over parts of Siberia and Canada, 2–3 times as large as in the simulations.

The AR4 models exhibit enhanced warming along the coast of the Arctic poleward of 65 °N that is not evident in the observations. This distinctive spatial signature is a prominent feature in both the historical simulations examined in this paper and in the climate projections for the 21st century (figures 10.8 and 10.9 in ref. (2)) and the IPCC Third Assessment Report (figure 9.10 in ref. (15)). That it is common to the runs with multiple forcings (Fig. 2) and to the runs with CO_2 forcing only (Fig. 5) indicates that it cannot have been induced by the seasonality in the simulated aerosols. That it is confined so close to the Arctic coast is suggestive of a localized amplification of the warming by feedbacks operating during the cold season that are overemphasized in the AR4 models. A more detailed seasonal breakdown of the patterns might shed additional light on the cause of this discrepancy.

The importance of the dynamical contribution to the pattern of the warming during the 1965–2000 reference interval is well-recognized (16, 17), but there does not exist a clear consensus as to how much of it should be regarded as a forced response to anthropogenic forcing and how much should be regarded as a reflection of the internal variability of the climate system. The qualitative similarity between the observed SLP trends and the SLP trends in the historical (1965–2000) and 2x CO_2 MMEM simulations shown in Fig. 3 is notable (see Fig. S2 for SLP changes in individual historical simulations). All three are characterized by a shift in the Northern and Southern Hemisphere annular modes toward their high-index polarity, indicative of poleward shifts in the extratropical storm tracks. Patterns of this form are consistent with theoretical expectations for the response to greenhouse warming (18, 19). However, in agreement with ref. (14) we find that the SLP trends in the MMEM of the 1965–2000 historical simulations are much smaller in absolute magnitude than the observed trends during this period.

The simulated wintertime warming over **N** (40–90 °N) is also much smaller than in the observations. Scaled as a fraction of the

of the rise in annual-mean GSST in Table 1, the dynamical component of the warming is over three times as strong in the observations as in the MMEM of the historical (1965–2000) simulations, and about twice as strong in the historical simulations as in MMEM of the 2x CO_2 runs. This 7 : 2 : 1 ratio is roughly comparable to the corresponding ratios for the wintertime 1965–2000 SLP trends shown in Fig. 3.

That the simulated SLP trends for the 1965–2000 reference period are so much smaller than observed has been attributed to the inability of the models to simulate the anthropogenically forced trends in the atmospheric circulation during this period (14). An alternative interpretation is that these SLP trends and the associated enhanced wintertime warming over **N** during this period are sampling fluctuations related to the variability of the coupled climate system (20). The circulation changes accompanying the shift toward the warm polarity of the ENSO cycle (or Pacific Decadal Oscillation) (21) in 1976–1977 project strongly upon the 1965–2000 SLP trend over the Pacific sector and contributed to the wintertime warming over Alaska and Canada (5–7). In a similar manner, the strengthening of the thermohaline circulation in the North Atlantic from the early 1970s onward favored a trend in the positive polarity of the North Atlantic Oscillation and warmer winters over high latitudes of Eurasia (22, 23). Over such short time intervals and restricted spatial domains, the variability generated by the internal dynamics of the climate system can overwhelm the anthropogenically forced variability (24). Hence, the failure of the models to simulate the full amplitude of the SLP trends and the associated warming over **N** during the 1965–2000 reference interval may be more a reflection of the inherent limitations in our ability to predict (or hindcast) the internal variability of the climate system than to an underestimate of the climate forcing or the models' sensitivity to it.

Whether the dynamical contribution to the wintertime warming over **N** should be regarded as anthropogenically induced or attributed to natural variability has important implications for inferences about climate sensitivity that rely on the historical record of climate change over the Northern Hemisphere. If the dynamical contribution to the warming over **N** were removed by performing a dynamical adjustment, it is evident from Table 1 that the seasonality of the warming over the Northern Hemisphere would be substantially reduced, along with the apparent high-latitude amplification of the warming (and the excess warming of land surface air temperature relative to sea surface temperature), and that the agreement between the historical simulations and observations would be substantially improved.

Materials and Methods

Climate Model Simulations. The simulations analyzed in this study are from a suite of climate models included in Phase 3 of the World Climate Research Programme (WCRP) Coupled Model Intercomparison Project (CMIP3) multimodel datasets (2), which were used in the IPCC AR4. The models are listed in Table S1. We consider only the simulations that include both the effects of stratospheric ozone depletion and sulfate aerosols injected into the stratosphere by explosive volcanic eruptions. Throughout this paper we use the term "trend" to denote linear trend as defined in terms of a conventional least-squares best fit. We express these linear trends as temperature changes over prescribed reference intervals (i.e., the difference in the linear trend line between the beginning of the interval and the end of the interval).

Climate Data. In this study we make use of the observational datasets listed in Table S2. The primary dataset is the National Climate Data Center merged land-ocean surface temperature analysis (MLOST, ref. (25)), with its land component [Global Historical Climatology Network, version 3 (GHCN3, ref. (26))], and ocean component [Extended Reconstructed Sea Surface Temperature, version 3b (ERSST3b, ref. (27)]. The SAT data are formatted on a uniform 5° latitude by 5° longitude global grid for the period of record: November 1919 through October 2008. We also analyze surface temperature datasets from HadCRUT3 (28) and GISTEMP (29), the results of which are presented in Table S3.

We use the SLP field from the National Oceanic and Atmospheric Administration (NOAA)/Cooperative Institute for Research in Environmental Sciences 20th Century Reanalysis (20CR), version 2 (30). The 20CR data were obtained from the NOAA/Office of Oceanic and Atmospheric Research/Earth System Research Laboratory, Physical Sciences Division (Boulder, CO) website at www.esrl.noaa.gov/psd/. The SLP data are formatted on a uniform 2° latitude by 2° longitude global grid for the time period November 1919 through October 2008. We have used this product not only because it is the only state-of-the-art SLP dataset that extends back to the early 20th century, but also because the spurious discontinuities in other reanalysis products that coincide with changes in the observing system could contaminate the time series of the adjustment. The 20CR should be free of such discontinuities because it is based on surface data only.

Our boreal cold season (November–April) extends across the divide between calendar years. Following the same convention used in dealing with the conventional winter season (December–February), we assign the cold season for year n and year $n+1$ to year $n+1$ (e.g., November 1964 through April 1965 to the calendar year 1965). Our boreal warm season is defined as May through October.

We remove the influence of the annual cycle by forming monthly-mean SAT and SLP anomalies, which are departures from the long-term calendar-month means.

Dynamical Adjustment. The dynamical adjustment methodology is based on partial least-squares (PLS) regression (31). Following the procedures illustrated in ref. (32), we applied PLS to adjust dynamically the time series of area-averaged SAT poleward of 40 °N (**N**, the "predictand") on the basis of the time-varying indices of spatial patterns in the SLP field poleward of 20 °N (the "predictors"). Here, PLS regression is performed by first correlating **N** with standardized SLP at each grid point poleward of 20 °N to form a one-point correlation map expressing the relationship between SLP and SAT averaged over **N**. Next, the monthly, standardized SLP field is projected onto the correlation pattern, weighting each grid point by the cosine of latitude, to obtain a time-varying index of the correlation pattern. This index is then regressed out of both **N** and the SLP field.

The above steps are repeated using the residual **N** time series and the residual SLP field until the successive cross-correlation patterns no longer explain an appreciable fraction of the variance of the area-averaged SAT time series. By construction, the predictor time series derived from the SLP field are mutually orthogonal. The decision of how many cross-correlation patterns to use as predictors of the reference time series is determined by cross-validation. We employed bootstrapping, leaving out the boreal cold-season months of one year (six monthly samples) as a validation set, using the remainder of the data as a training set, and predicted the validation set SAT samples by projecting the validation set SLP samples onto cross-correlation patterns developed from the training set SAT and SLP data. This procedure was repeated for each year to obtain an independent prediction of the area-averaged SAT time series (**N**). As the number of PLS regression passes (i.e., the number of cross-correlation patterns used) is increased, the correlation between the predicted time series **N** and the cross-validated predictor time series levels off, indicating that the point of diminishing returns has been reached.

Observational and model SAT data for the boreal cold season 1920 through 2008 were dynamically adjusted using PLS regression with only two passes, a conservative choice based on the aforementioned cross-validation procedure, which showed modest increases in the correlation between **N** and the cross-validated predictor time series out to four passes.

The dynamically adjusted MMEM SAT time series were produced by averaging the adjusted SAT time series in individual runs, first across each model's ensemble members and then across all of the models.

ACKNOWLEDGMENTS. J.M.W. and B.V.S. were supported by the Climate Dynamics Program Office of the National Science Foundation under Grant 0812802. Q.F., P.L., and C.M.J. were supported by the National Basic Research Program of China (2012CB955303), National Aeronautics and Space Administration Grant NNX08AG91G, and National Oceanic and Atmospheric Administration Grant NA08OAR4310725.

1. Randall DA, et al. (2007) Climate models and their evaluation. *Climate Change 2007: The Physical Science Basis*, eds S Solomon et al. (Cambridge University Press, New York), pp 589–662.

2. Meehl GA, et al. (2007) Global climate projections. *Climate Change 2007: The Physical Science Basis*, eds S Solomon et al. (Cambridge University Press, New York), pp 747–845.

3. Thompson DWJ, Wallace JM, Hegerl G (2000) Annular modes in the extratropical general circulation. Part II: Trends. *J Clim* 13:1018–1036.
4. Quadrelli R, Wallace JM (2004) A simplified linear framework for interpreting patterns of Northern Hemisphere wintertime climate variability. *J Clim* 17:3728–3744.
5. Trenberth KE, Hurrell JW (1994) Decadal atmosphere-ocean variations in the Pacific. *Clim Dyn* 9:303–319.
6. Graham NE (1994) Decadal-scale climate variability in the tropical and North Pacific during the 1970s and 1980s: Observations and model results. *Clim Dyn* 10:135–162.
7. Zhang Y, Wallace JM, Battisti DS (1997) ENSO-like interdecadal variability: 1900–1993. *J Clim* 10:1004–1020.
8. Wallace JM, Zhang Y, Renwick JA (1995) Dynamical contribution to hemispheric mean temperature trends. *Science* 270:780–783.
9. Wallace JM, Zhang Y, Bajuk L (1996) Interpretation of interdecadal trends in Northern Hemisphere surface air temperature. *J Clim* 9:249–259.
10. Hurrell JW (1996) Influence of variations in extratropical wintertime teleconnections on Northern Hemisphere temperatures. *Geophys Res Lett* 23:665–668.
11. Broccoli AJ, Lau NC, Nath MJ (1998) The cold ocean-warm land pattern: Model simulation and relevance to climate change detection. *J Clim* 11:2743–2763.
12. Gillett NP, Thompson DWJ (2003) Simulation of recent Southern Hemisphere climate change. *Science* 302:273–275.
13. Deser C, Phillips AS (2008) Atmospheric circulation trends, 1950–2000: The relative roles of sea surface temperature forcing and direct atmospheric radiative forcing. *J Clim* 22:396–413.
14. Gillett NP, Zwiers FW, Weaver AJ, Stott PA (2003) Detection of human influence on sea-level pressure. *Nature* 422:292–294.
15. Cubasch U, et al. (2001) Projections of future climate change. *Climate Change 2001: The Scientific Basis* (Cambridge University Press, New York), pp 526–582.
16. Folland CK, et al. (2007) Observed climate variability and change. *Climate Change 2007: The Physical Science Basis*, eds S Solomon et al. (Cambridge University Press, New York), pp 99–181.
17. Sutton RT, Dong B, Gregory JM (2007) Land/sea warming ratio in response to climate change: IPCC AR4 model results and comparison with observations. *Geophys Res Lett* 34:L02701.
18. Lu J, Vecchi GA, Reichler T (2007) Expansion of the Hadley cell under global warming. *Geophys Res Lett* 34:L06805.
19. Frierson DMW, Lu J, Chen G (2007) Width of Hadley cell in simple and comprehensive general circulation models. *Geophys Res Lett* 34:L18804.
20. DelSole T, Tippet MK, Shukla J (2011) A significant component of unforced multidecadal variability in recent acceleration of global warming. *J Clim* 24:909–926.
21. Mantua NJ, Hare SR, Zhang Y, Wallace JM, Francis RC (1997) A Pacific interdecadal climate oscillation with impacts on salmon production. *Bull Am Meteorol Soc* 78:1069–1079.
22. Semenov VA, Latif M, Jungclaus JH, Park W (2008) Is the observed NAO variability during the instrumental record unusual? *Geophys Res Lett* 35:L11701.
23. Semenov VA, et al. (2010) The impact of North Atlantic-Arctic multidecadal variability on Northern Hemisphere surface air temperature. *J Clim* 23:5668–5677.
24. Deser C, Knutti R, Solomon S, Phillips AS (2012) Communication of the role of natural variability in future North American climate. *Nat Clim Change*, in press.
25. Smith TM, Reynolds RW, Peterson TC, Lawrimore JH (2008) Improvements to NOAA's historical merged land-ocean surface temperature analysis (1880–2006). *J Clim* 21:2283–2296.
26. Lawrimore JH, et al. (2011) An overview of the Global Historical Climatology Network monthly mean temperature data set, version 3. *J Geophys Res* 116:D19121.
27. Smith TM, Reynolds RW (2004) Improved extended reconstruction of SST (1854–1997). *J Clim* 17:2466–2477.
28. Brohan P, Kennedy JJ, Harris I, Tett SFB, Jones PD (2006) Uncertainty estimates in regional and global observed temperature changes: A new dataset from 1850. *J Geophys Res* 111:D12106.
29. Hansen J, Ruedi R, Sato M, Lo K (2008) Global surface temperature change. *Rev Geophys* 48:RG4004.
30. Compo GP, et al. (2011) The twentieth century reanalysis project. *Q J R Meteorol Soc* 137:1–28.
31. Abdi H (2010) Partial least squares regression and projection on latent structure regression (PLS regression). *Wiley Interdiscip Rev Comput Stat* 2:97–106.
32. Smoliak BV, Wallace JM, Stoelinga MT, Mitchell TP (2010) Application of partial least squares regression to the diagnosis of year-to-year variations in Pacific Northwest snowpack and Atlantic hurricanes. *Geophys Res Lett* 37:L03801.